ChemistrySelect
Chemistry Europe
European Chemical Societies Publishing

RESEARCH ARTICLE

Plant-Derived Nanoparticles for Advanced Ni–P–TiO_2 Composite Coatings on AH36 Marine Steel

Ganta Suresh[1] | T. Vinod Kumar[1] | R. Muraliraja[1] | A. Padmapriya[2] | J. Rajasekar[3] | S. Arunkumar[1]

[1]Department of Mechanical Engineering, Vels Institute of Science Technology and Advanced Studies, P.V. Vaithiyalingam Road, Chennai, Tamil Nadu, India | [2]Department of Chemistry, School of Arts and Science, Vinayaka Mission's Research Foundation (DU), Chennai Campus, Paiyanoor, Chennai, Tamil Nadu, India | [3]Department of Mechanical Engineering, Sri Ganesh College of Engineering and Technology, Puducherry, India

Correspondence: T. Vinod Kumar (vinod.se@vistas.ac.in) | R. Muraliraja (muralimechraja@gmail.com)

Received: 6 August 2025 | **Revised:** 8 December 2025 | **Accepted:** 22 December 2025

Keywords: AH36 steel | composite coatings | corrosion | marine environment | strength

ABSTRACT

The synthesis of electroless Ni–P–TiO_2 composite coatings on marine grade AH36 steel was done using plant-extract-derived titanium dioxide nanoparticles in the present work. TiO_2 nanoparticles were synthesized using *Indigofera tinctoria* extract as an efficient reducing and capping agent by the green method. Anatase, rutile, and amorphous polymorphs were obtained by controlled temperature calcinations and characterized using scanning electron microscopy (SEM) and X-ray diffraction (XRD). They were then dispersed in a premixed bath of electroless Ni–P (including sodium hypophosphite, ammonium chloride, and sodium tri-citrate) with the zwitterionic surfactant for enhanced particle dispersion. One hybrid composite and three single-phase TiO_2 composites with different contents were coated at 85°C for 1 h. The coated samples presented a homogeneous structure in sizes of grain with apparent improvement in microhardness and improved corrosion resistance. A higher TiO_2-added composite coating shows well-defined surface features, as well as superior electrochemical performance. Thickness of the coating was correlated with the phase and elemental composition of particles. The Tafel test showed a marked reduction in the corrosion current density and an increase of anti-corrosion for marine environments. It can be presumed that the green synthesis of Ni–P–TiO_2 is a multilayer, promising economical and environment-friendly approach for enhancing the corrosion resistance and durability of AH36 marine steel.

1 | Introduction

Demand has significantly changed for high-performance protective coatings for marine steel in the last decade. The requirement for high-performance coatings applied to marine-grade steels has increased significantly over the last 10 years in response to increasing concerns of aggressive seawater environments, biofouling, and long-term mechanical degradation. AH36 steel, a high-strength, low-alloy structural steel, is widely used in shipbuilding and offshore engineering, such as ship hulls, offshore platforms, ocean engineering equipment, and deep-sea structure components, which can suffer from pitting failures due to chloride attack in the marine environment [1]. The degradation not only applies to the safety of structures but also results in higher maintenance costs and longer downtimes. Conventional organic and galvanized coatings and corrosion inhibitors could offer only partial (for a limited time period) protection. However, with the growing adoption of tougher environmental regulations and to meet higher performance criteria, a sustainable surface-modification technology with high-performance durable coatings is required [2]. Attention has also been paid to electroless nickel–phosphorus (Ni–P) deposits as an alternative plating process that can be used in place of other electroplating methods because they can generate uniform, nonporous and metallurgically bonded

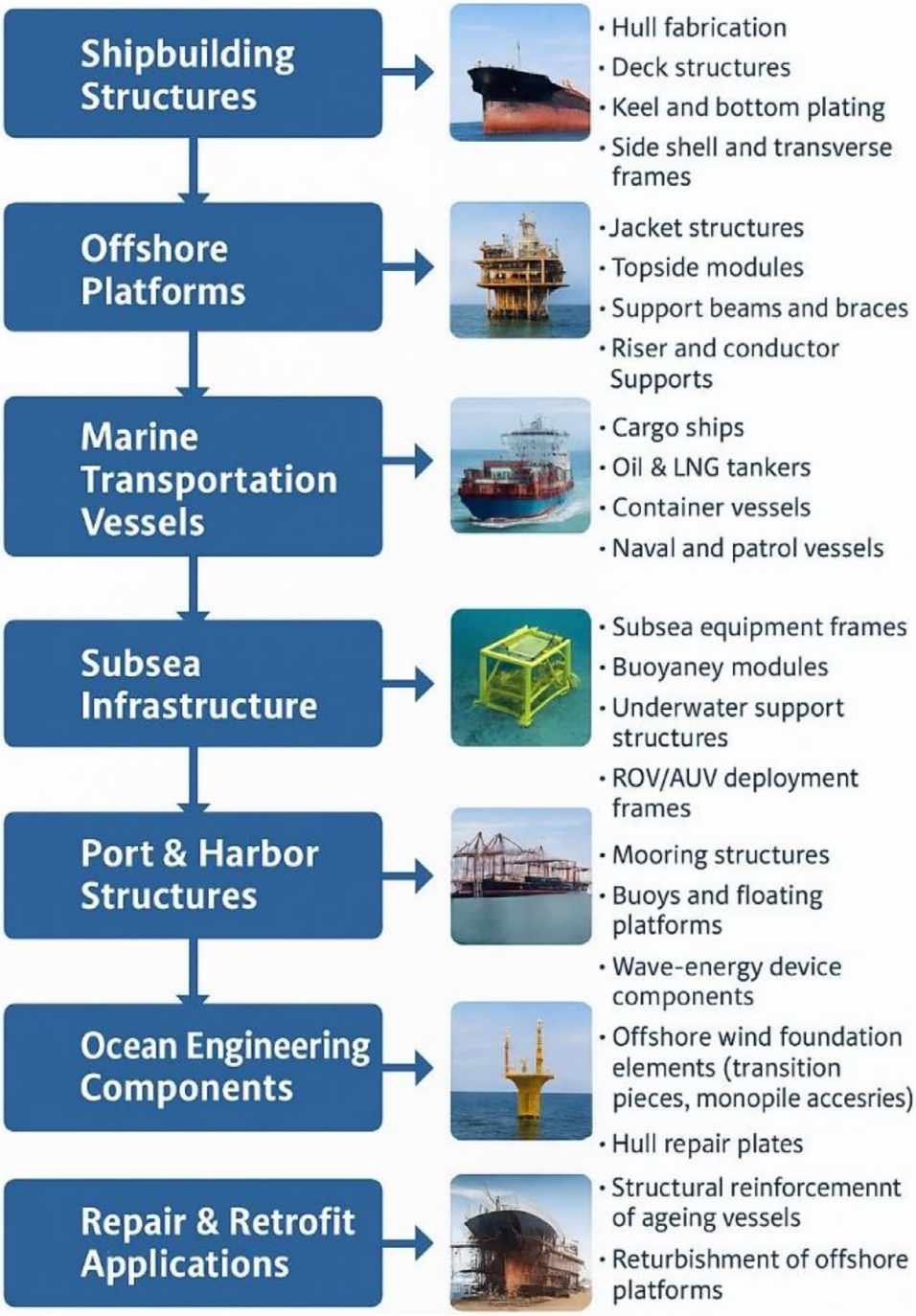

FIGURE 1 | Applications of AH36 steel in the marine environment.

coatings on complex-shaped geometries without exerting an external electric current. It has been reported that the presence of ceramic nanoparticles (such as TiO_2, Al_2O_3, and SiC) in the Ni–P matrix can significantly increase the hardness of crystals, wear resistance, and corrosion resistance through its particle dispersion strengthening and hinder properties [3]. In particular, TiO_2 is widely studied owing to its good chemical inertness, photocatalytic activity, biocompatibility, and the ability of promoting the reinforcement effect in the Ni–P matrix. However, traditional chemical routes for the synthesis of TiO_2 nanoparticles might be associated with the use of toxic precursors, energy-intensive processes, and environmentally harmful by-product [4]. This has led to the development of the green route of synthesis using plants extract for biodegradable, cheap, and eco-friendly substitutes as natural sources of a reducing and capping agent. The present test showed that these plant-derived nanoparticles yield a lower environmental impact and possibly enhance the performance of coating due to better surface chemistry functionalization and dispersion properties.

Latest advancements in electroless composite coating technology are considered to offer possible improvement in microstructure characteristics, namely mechanical and anticorrosion properties, by controlled addition of nanoparticle filler material. For

instance, Shahzad et al. [4] revealed that electroless Ni–P–Ti coatings exhibited higher microhardness and superior corrosion resistance than the monolithic Ni–P in the homogeneous distribution of nanoparticles and better interfacial bonding between particles and matrix. Shozib et al. [5] applied machine-learning and response-surface techniques to develop an optimal coating process while revealing the significance of nanoparticle concentration, pH, as well as the influence of the surfactant level on the deposition rate, microhardness, and roughness. Similarly, Selvan et al. [6] studied the electroless deposition of the Ni–P–TiO_2 coating process on AH36 steel and observed that the surface roughness of the deposited coating increased and adhesion strength enhanced with increasing bath constituents. These works, when taken together, reveal that the structure–property relationship of electroless Ni–P–TiO_2 coatings is reasonably linked to phase composition, particle size, and thereby suspension stability, as well as bath chemistry. For instance, rutile and anatase TiO_2 phases offer distinct mechanical hardening due to finer anatase phase crystallinity and higher resistance in chloride-containing environments for the rutile phase. Hao et al. [7] also highlighted the effects of deep-sea environmental conditions (high-pressure, salinity, and dissolved oxygen level) on material deterioration and stressed the need for strong surface engineering solutions among which Ni–P-based nanocomposite is one of the good candidates. These are part of a trend described for multifunctional coatings that can be tested against corrosion, erosion, biofouling, and mechanical wear at the same time, because this is possible with structural steels used in marine and offshore applications. Nevertheless, problems still persist with respect to "coating the nanoparticles uniformly over a large area and controlling their thickness on the surface of the substrate, as well as suppressing particle coalescence and stabilizing the solution" during long-term deposition. In this study, an attempt has been made to overcome these shortcomings by undertaking our current investigation with emphasis on the optimization of electroless bath formulations and on the implementation of surfactant systems for the improvement of performances using hybrid nanoparticle phases. Zhu et al. [8] have used Taguchi grey relational analysis for optimizing the process parameters in surface-engineering processes, showing its utility for multi-response optimization during electroless coating. Vijayanand et al. [9] have shown that surfactant plays a crucial role in the particle distribution, porosity, and hardness of coating. Salicio-Paz et al. [10] pointed out that the electroless solution must be fully optimized when low-phosphorus Ni–P coatings were needed. These enhancements in methodology are essential because the pH, temperature, and reducing agent concentration effects are significant for electroless Ni–P-TiO_2 coatings, particularly when using green-synthesized nanoparticles that might exhibit irregular morphologies and/or surface functional groups. The applications of AH36steel in the marine environment, in general, are divided into several categories presented in Figure 1.

In this regard, the incorporation of plant-mediated TiO_2 nanoparticles in Ni–P matrices might be an alternative solution for synthesizing sustainable and high-performance coatings due to the excellent physiochemical properties obtained from natural extracts such as effective dispersion stability and peculiar surface chemistry [11–13]. The schematic representation of the present research work is represented in Figure 2.

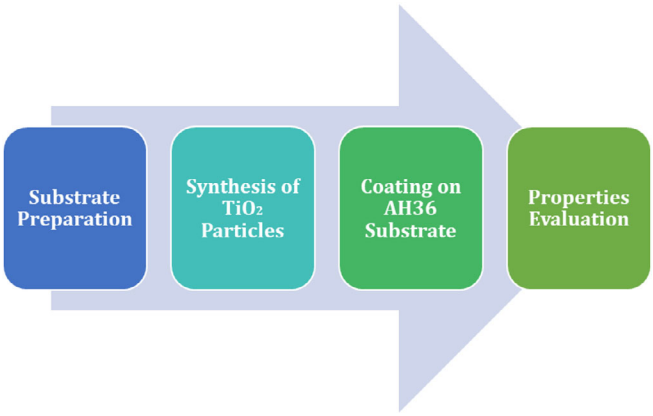

FIGURE 2 | Schematic representation of the flow of this research work.

TABLE 1 | Chemicals required for the pretreatment process.

S. No.	Required chemicals	Purpose
1	Sulfuric acid	Activating the surface
2	Acetone	Removing the impurities
3	Ethanol	Degreasing the substrate
4	Nitric acid	Cleaning the beakers

In addition, the combination of anatase, rutile, and amorphous TiO_2 phases allows for the development of hybrid coatings with a compromise between mechanical and corrosion resistance. Considering the current trend to use AH36 steel in offshore structures and at the same time the growing demand for environmentally friendly coating technologies, this study opens a new window on green-sourced Ni–P–TiO_2 composite coatings that can be used to provide long-term corrosion resistance and improved structural integrity. As such, as a systematic comparative study, this work aims at synthesizing TiO_2 using plant extracts, adding the particles to electroless Ni–P, and examining the influence of its phase composition on microhardness, coating thickness, morphology, and corrosion potentials of AH36 steel used in the marine environment.

2 | Experimental Details and Procedures

2.1 | Materials and Substrate Preparation

AH36 naval-grade steel was obtained from the Indian Navy reprocessing unit and cut as rectangular specimens to appropriate size. The steel's certified chemical composition was as follows: 0.17 wt% C, 1.22 wt% Mn, 0.017 wt% Ti, 0.012 wt% P, 0.39 wt% Si, 0.042 wt% Al, 0.016 wt% Cu, and 98.13 wt% Fe. All chemicals were of analytical grade (Table 1) and the surface was pretreated. The samples were polished using emery papers of different grades, de-greased by ethanol, and cleaned ultrasonically. Before coating, substrates were soaked in sulfuric acid for surface activation and then washed with acetone to remove organic contaminants. The glassware was cleaned with nitric acid to prevent contamination [14]. The cleaned and activated steel specimens were dried in warm air, and then the electroless deposition took place.

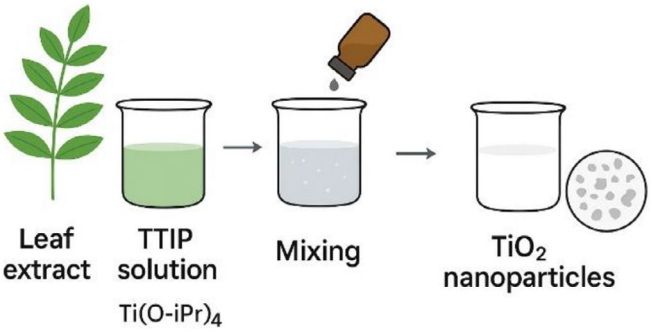

FIGURE 3 | Schematic representation of synthesis of TiO_2 nanoparticles.

2.2 | Synthesis of TiO_2 Nanoparticles Using the Plant Extract

TiO_2 nanoparticles were prepared through the green chemistry method using the extract of *Indigofera tinctoria* as a natural reducing and capping agent. Shade-dried and freshly plucked leaves were soaked overnight in distilled water, followed by boiling to achieve the plant extract. TIP was used as the titanium donor. The plant extract solution was slowly poured into a 100-mL beaker of TIP and stirred constantly throughout the procedure at room temperature. Change in color from white to yellowish gray indicated the formation of TiO_2 nanoparticles. The solid precipitate was filtered, and then the obtained precipitation was dried at 110°C to get a powder that was then calcined at 500°C for anatase TiO_2 or at 800°C for rutile-phase nanoparticles [15]. A third set was left without high-temperature treatment to get amorphous TiO_2. The anatase, rutile, and amorphous TiO_2 phases were confirmed by the scanning electron microscopy (SEM) and X-ray diffraction (XRD) methods. The preparation process of nanoparticles is shown in Figure 3.

TiO_2 nanoparticles were prepared in three stages and examined by SEM and shown in Figure 4. An XRD analysis was performed in order to confirm the crystal form of TiO_2 within the EL Ni–P deposit. Patterns indicated the presence of various TiO_2 polymorphs—anatase, rutile, and amorphous—in the samples. The characteristic peaks of anatase TiO_2 samples at around 2θ value, for example, the [1 0 1], [0 0 4], and [2 0 0] planes, were sharply occurred at 25.3°, 37.8°, and 48° with high crystallinity, respectively. Rutile samples had strong peaks at around 27.4°, 36.1°, and 54.3° ascribed to the [1 1 0], [1 0 1], and [2 1 1] planes, which confirmed the rutile crystalline structure [16]. In contrast, amorphous TiO_2 samples exhibited broad weak peaks indicating low crystallinity (Figure 5).

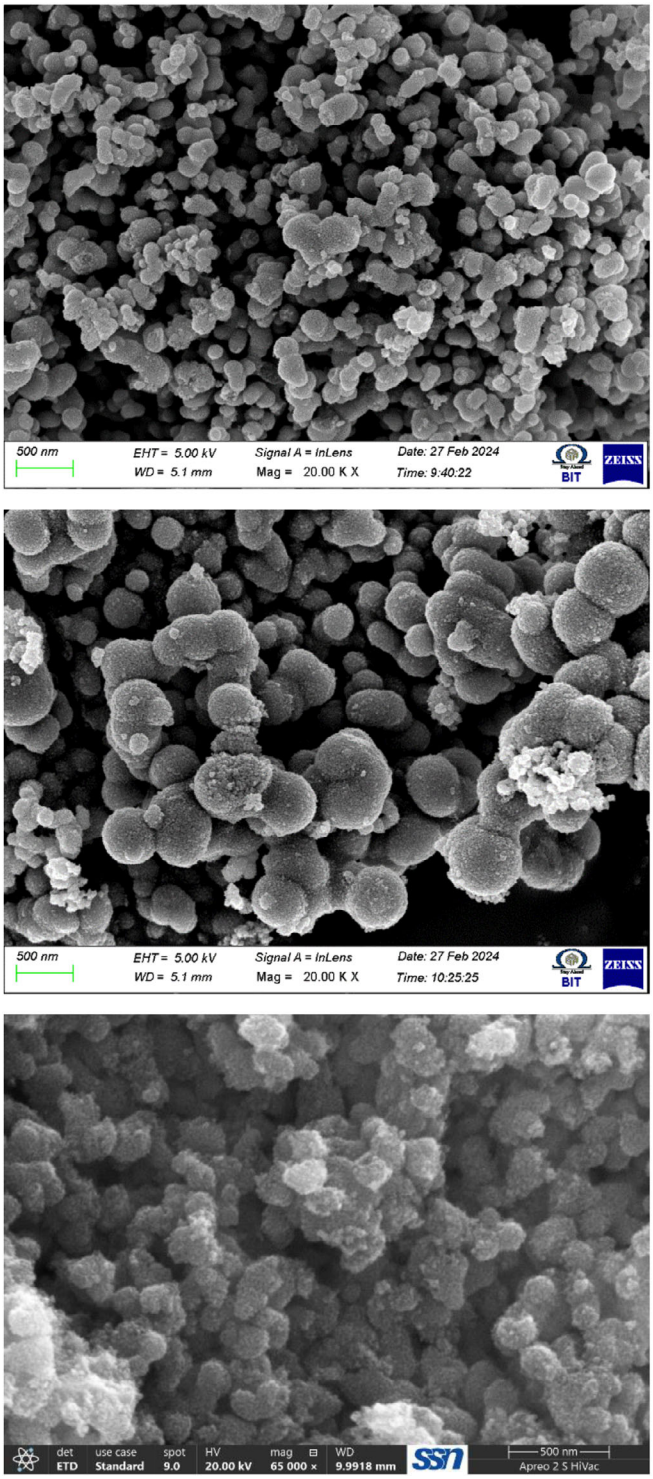

FIGURE 4 | SEM images of TiO_2: (a) anatase, (b) rutile, and (c) amorphous.

2.3 | Preparation of the Electroless Ni–P–TiO_2 Plating Bath

The electroless plating solution was prepared with nickel sulfate as a metal source, sodium hypophosphite as a reducing agent, trisodium citrate as a complexing agent, and ammonium chloride as a stabilizer (as listed in Table 2). The bath pH was adjusted using liquid ammonia. All chemicals were of analytical grade and dissolved in 1-L distilled water. The bath was heated to 85°C and kept at this temperature during the deposition. The zwitterionic surfactant (0.018 g/L) was prepared independently, for improving the dispersion of nanoparticles. Five drops of this surfactant solution were added to the main bath after the reduction reaction started. The TiO_2 nanoparticles were mixed in the electrolyte using magnetic stirring to avoid agglomeration and ensure even mixing [17–19].

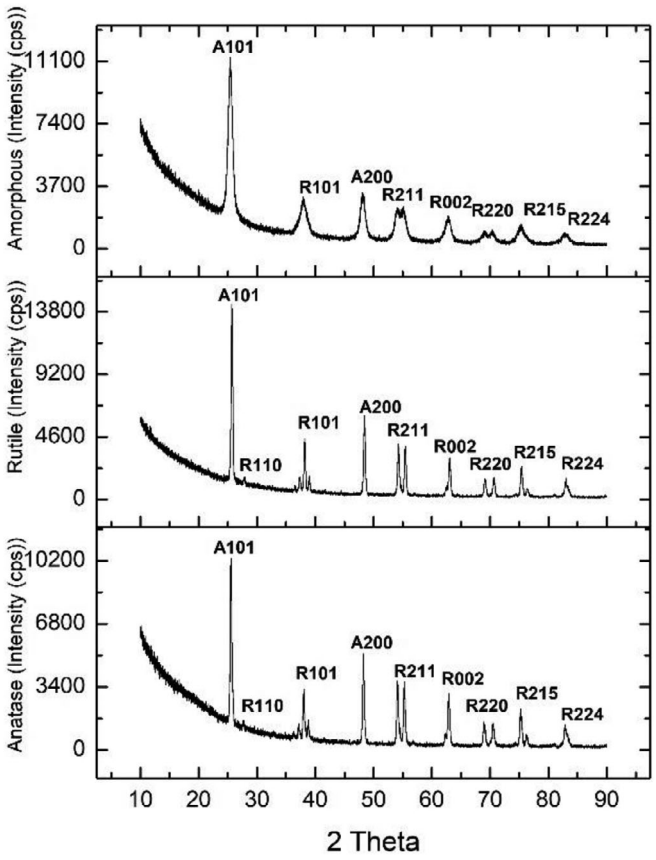

FIGURE 5 | X-ray diffractogram of various phases of TiO_2 particles.

TABLE 2 | Chemicals required for the preparation of electrolyte.

S. no.	Required chemicals to be purchased	Quantity	Purpose
1	Sodium hypophosphite	40 g	Reducing agent
2	Sodium tri-citrate	50 g	Complexing agent
3	Ammonium chloride	50 g	Regulator
4	Liquid ammonia	As required	pH
5	Nickel sulfate	30 g	Ni source

2.4 | Electroless Deposition of Ni–P–TiO_2 Coatings and Its Characterization Techniques

Coatings were performed in 250-mL glass beakers with the electroless bath at 85°C without agitating the etched steel substrates, except for a magnetic stirring that was used to maintain TiO_2 particles suspended. Table 3 shows the composition of the samples developed using the electroless deposition of Ni–P–TiO_2 coatings.

After deposition, samples were rinsed with distilled water, dried, and stored in desiccators prior to characterization. Coating thickness (T) was calculated as

$$T = \frac{w \times 10^4}{dA} \quad (1)$$

TABLE 3 | Composition of the samples developed using the electroless coating process.

Description	Composition
Sample 1 (S1)	Ni–P–TiO_2 (rutile 0.1 g)
Sample 2 (S2)	Ni–P–TiO_2 (amorphous 0.1 g)
Sample 3 (S3)	Ni–P–TiO_2 (anatase 0.1 g)
Sample 4 (S4)	Ni–P–TiO_2 (rutile 0.05 g + amorphous 0.05 g + anatase 0.05 g) hybrid

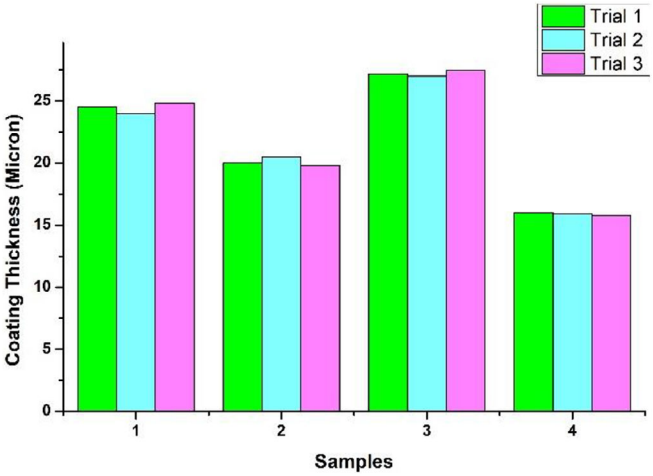

FIGURE 6 | Coating thickness of the deposits.

where T is the coating thickness (μm), w is the weight gain (g), d is the density of the deposit (g/cm^3), and A is the surface area of deposition (cm^2). The surface morphology of coatings was assessed using a SEM, specifically the Hitachi Model S-3400N, operated at an accelerating voltage of 15 kV. Elemental analysis of the deposits was conducted with an attached EDS system. XRD with a Rigaku Ultima IV diffractometer with a copper anode was used to identify phases and structures. XRD patterns were recorded in the 2θ region from 10° to 90° using a step size of 0.02° and time base per second. The anticorrosion behavior of the coatings in a 3.5 wt% NaCl solution was investigated using linear polarization experiments and XRD analysis. The working electrode (substrate) surface was maintained to 1 cm^2. The counter electrode was a graphite rod, and the reference electrode was a saturated calomel electrode. At first, the open circuit potential (OCP) was recorded, and then a potentiodynamic polarization scan was performed at 1 mV/s in the positive direction. The electrodes were left for 30 min in the electrolyte to reach a steady OCP before the measurements of potential. Current and potential were also recorded at the same time, and the data obtained were used to plot Tafel curves for corrosion study.

3 | Results and Discussions

The coating thickness measurements indicated that the sample 3 (Ni–P–TiO_2-anatase phase) had the highest value of deposited coating as illustrated in Figure 6. Such an excellent growth property is attributed to the inherent nature of anatase TiO_2 with higher surface energy, smaller grain size, and better catalysis

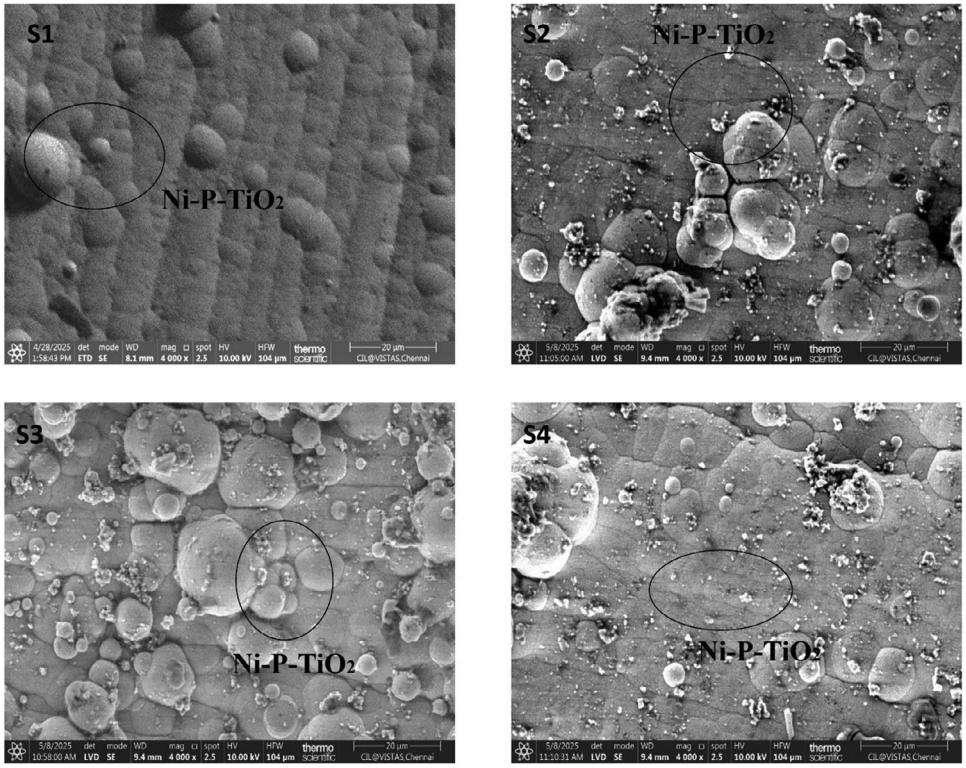

FIGURE 7 | Surface morphology of the prepared samples.

performance than that of rutile and amorphous phases. These characteristics greatly promote the nucleation of Ni–P in the electroless process, resulting in an accelerated deposition and a thicker composite layer. The dispersion of anatase particles was more stable in the synthetic bath, facilitated by the zwitterionic surfactant, ensuring particle availability at a substrate solution interface during coating to ascertain uniform disposition from leading to trailing edges over all durations of deposition [20, 21]. In comparison, S1 or S2 was less thick, because the rutile (S1) and amorphous TiO_2 (S2) were less reactive materials and played a smaller role in the catalytic reduction of the nickel ion. In the case of that hybrid sample (S4), all three phases were present and the interaction among particles probably conditioned theirs optimal contribution separately; as a result, their thickness remained moderate and did not exceed S3 either.

The SEM analysis of the electroless Ni–P–TiO_2 composite coatings as shown in the Figure 7 revealed distinct morphological differences among the samples, primarily influenced by the phase of TiO_2 incorporation and its corresponding elemental composition. All coatings displayed uniform deposition without cracks, indicating good bath stability and effective surface pretreatment. However, variations in surface texture, cluster distribution, and particle incorporation were clearly visible across samples S1–S4. Sample 1 (rutile TiO_2) showed a relatively smooth surface with moderately dispersed particles, corresponding to its composition of 89.5 wt% Ni, 9.62 wt% P, and 0.88 wt% TiO_2. The slightly higher P content contributed to a smoother, less nodular structure, as phosphorus tends to reduce surface roughness by promoting the formation of the amorphous Ni–P matrix. In contrast, Sample 2 (amorphous TiO_2), containing 89.2 wt% Ni, 9.91 wt% P, and 0.89 wt% TiO_2, exhibited a finer but more compact morphology.

TABLE 4 | Elemental composition of developed coated samples.

Sample ID	Ni (wt%)	P (wt%)	TiO_2 (wt%)
S1	89.5	9.62	0.88
S2	89.2	9.91	0.89
S3	89.8	9.25	0.95
S4	90.12	8.78	1.1

The highest P percentage among all samples led to increased amorphous character and reduced grain boundary definition, which is typical of high-phosphorus electroless coatings. Sample 3 (anatase TiO_2), with 89.8 wt% Ni, 9.25 wt% P, and 0.95 wt% TiO_2, presented the most prominent nodular structure and enhanced surface roughness. The composition of elements present in the deposit is attained using EDAX analysis and is listed in Table 4. The mapping of images used in this study is depicted in Figure 8 for Sample 3. The slightly lower P content and highest TiO_2 incorporation promoted heterogeneous nucleation sites, resulting in well-defined clusters that correlate with the increased catalytic activity of anatase [22]. This morphology supports thicker deposition and improved hardness, consistent with the coating thickness trends observed. The hybrid sample (S4), containing the highest TiO_2 content (1.1 wt%) and 90.12 wt% Ni with 8.78 wt% P, displayed dense, uniformly distributed nodules. The reduced phosphorus level favored a more crystalline Ni–P matrix, while the mixed TiO_2 phases enhanced particle dispersion. The SEM features confirm that higher TiO_2 incorporation and lower P levels increase nodularity and surface definition, illustrating the strong interplay between composition and microstructural evolution in Ni–P–TiO_2 coatings.

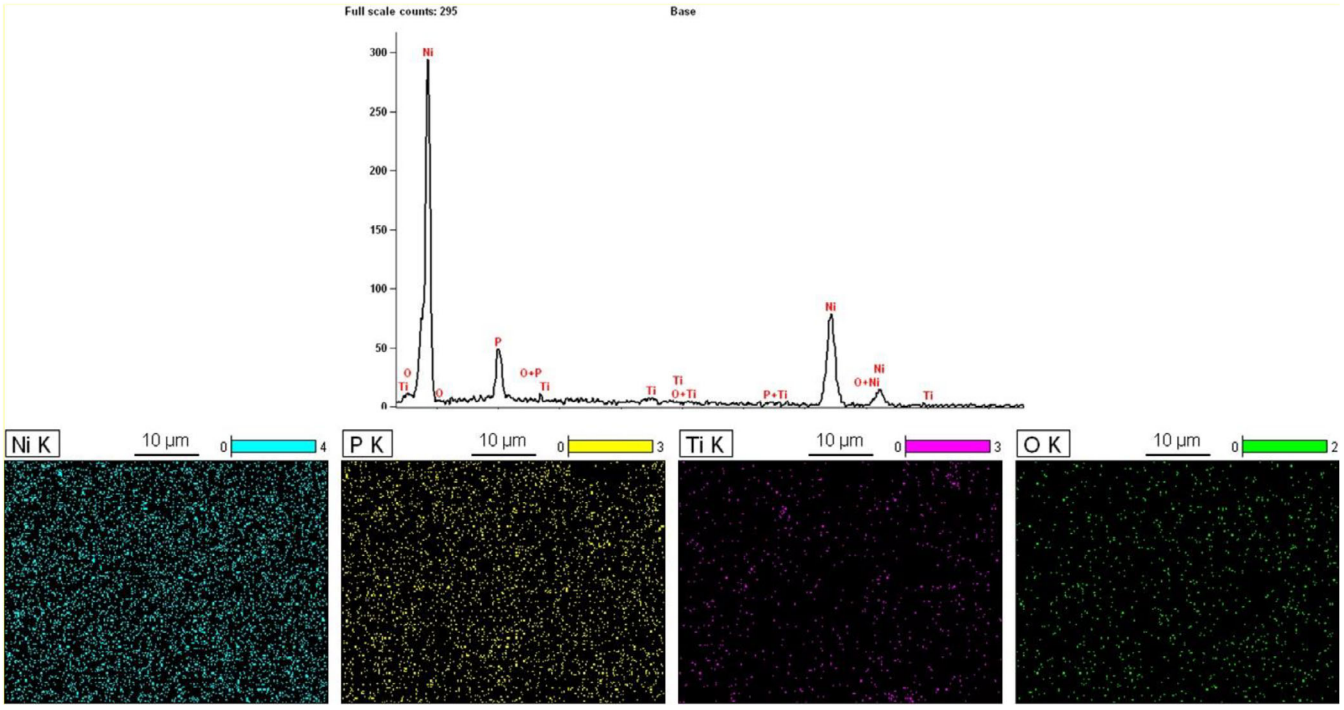

FIGURE 8 | Elemental analysis using mapping techniques for the Sample S3.

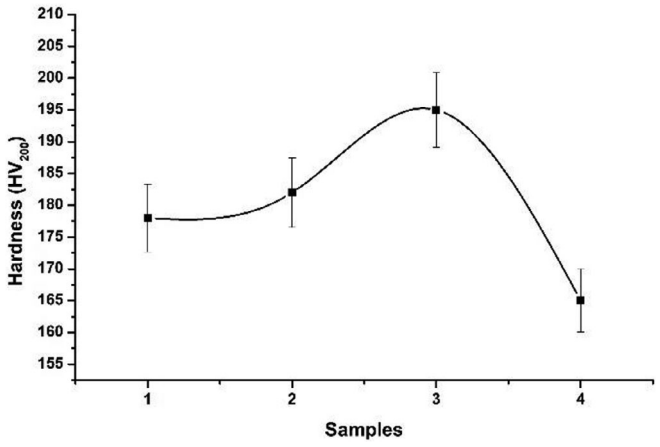

FIGURE 9 | Microhardness value of the deposits.

The microhardness measurement of the electroless Ni–P–TiO_2 composite coatings indicated considerable differences in hardness values for different types of TiO_2 phases embedded into the Ni–P matrix (Figure 9). The hardness of the coated samples was greater than that for the uncoated AH36 steel, which indicated the reinforcing effect of TiO_2 nanoparticles and the inherent enhancement of the Ni–P alloy system. The excellent microhardness of Sample 3 (anatase TiO_2) among the four samples well coincided with its increased coating thickness and the unique nodular surface morphology as observed in Figure 9. The increased hardness of S3 can be attributed to the fact that the finer crystallite size and higher surface reactivity of anatase TiO_2 facilitate a more effective interfacial bond as well as uniform dispersion in the Ni–P matrix. This leads to a higher dislocation motion barrier network, enhancing hardness. Sample 4 (hybrid TiO_2 mixture) also showed higher hardness than S1 and S2 due to higher incorporation of TiO_2 (1.1 wt%). Synergetic reinforcement results from the multi-TiO_2 phase as the combined function of anatase, rutile, and amorphous particles facilitates load transferring and microstructure compactness. Still, its hardness is slightly less than that of S3 in the big particle size range because of the wider particle size distribution and interphase interactions between sectile and trigonal grains, which can prevent more favorable close packing. Samples 1 (rutile TiO_2) and 2 (amorphous TiO_2) showed similarly lower but still enhanced hardness data. Rutile is also of quite low reactivity (and much more stable) and so it does not disperse very well, and amorphous TiO_2 with no real structure provides little strength. Additionally, the higher phosphorus content of rutile is responsible for a more amorphous Ni–P matrix that has been found to lower hardness than those with medium P or low-P deposits [23, 24].

Electrochemical corrosion of metallic systems is controlled by the kinetics of anodic metal dissolutions and cathodic reduction reactions that take place at the interface between the metal and electrolyte. These reactions have been studied by means of the potentiodynamic polarization (Tafel) method that is commonly used for the assessment of the corrosion resistance behavior of both coated and uncoated steels. The Tafel plot provides the main parameters, including corrosion potential (E_{corr}) and corrosion current density (I_{corr}), that act as a direct indication of the thermodynamic stability factor, and the kinetic corrosion rate of respective methods can be represented as shown in Figure 10. Corrosion potential is a measure of the propensity for anodic or cathodic reactions to occur, with more positive E_{corr} values indicating higher nobility of the surface. The I_{corr}, derived from the intersection of the anodic and cathodic Tafel slopes, provides a measure of the electron transfer rate and consequently the rate of material loss. The smaller the I_{corr}, the slower the

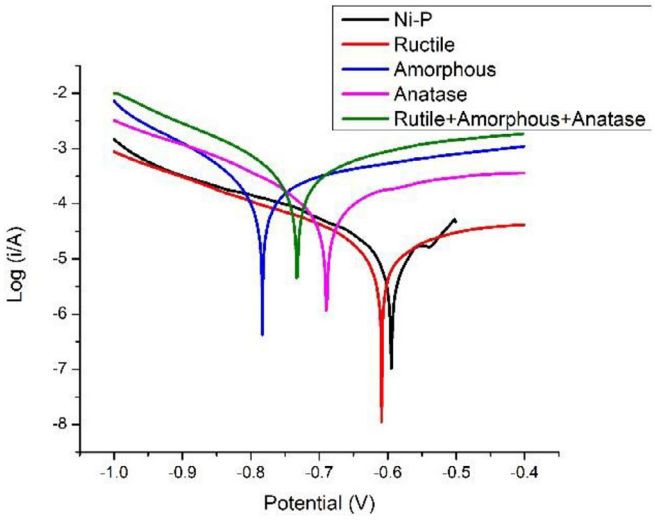

FIGURE 10 | Corrosion analysis of the samples using Tafel plot.

corrosion rate and the better the passivation and protective performance of the coating. In general, XPS and EIS results were in agreement with the microstructural characterization of the electroless Ni–P and Ni–P–TiO_2 composite coatings listed in Table 5, suggesting that the addition of TiO_2 nanoparticles can play an important role in a sense of changing the corrosion behavior by altering the microstructure as well as particle dispersion and barrier properties. The TiO_2 phase is important for control thickness, porosity, and catalytic activity of the coatings [25]. For instance, the anatase phase has a higher surface energy and smaller crystallite size, which facilitates better nucleation during deposition, resulting in densely packed and homogenous coatings. The more stable and chemically inert phase of rutile promotes better passivation and lower electron mobility, which makes it particularly efficient in chloride-containing media. Amorphous TiO_2 does not have a crystalline structure and cannot provide as much reinforcement as its crystalline counterparts. The above calculation was inferred from the Tafel plot and indicates that corrosion parameters in this work well describe the impact of TiO_2 phases on electrochemical properties. The most positive values of E_{corr} (−0.59 V) and the lowest ones for I_{corr} (1.6×10^{-8} A/cm^2), represented as very low CR = 0.00019 mm/year, were recorded on rutile TiO_2. It is an indication of excellent corrosion resistance and strong passivation properties. Anatase-loaded coatings showed quite a positive value of E_{corr} (−0.70 V) and low I_{corr} (1.6×10^{-6} A/cm^2) with a corrosion rate of 0.019 mm/year, which ensures that enhancement in barrier properties is realized compared to the Ni–P alone. On the other hand, amorphous TiO_2 gave (−0.79 V) E_{corr} value much farther negative and high I_{corr}, 1.0×10^{-5} A/cm^2, which resulted in the highest corrosion rate of 0.12 mm/year. These findings reveal that the amorphous TiO_2 has a limited structural reinforcement effect on the Ni–P matrix and little is obtained in anti-corrosion properties. The high $TfiO_2$ content in the hybrid TiO_2 coating did not really influence its E_{corr}, which was −0.74 V; I_{corr} of 1.25×10^{-5} A/cm^2, or the corrosion rate o 0.15 mm/year [26]. This implies that mixed phases could introduce the excessive particle–particle interaction, which cancels out the synergy effect.

4 | Conclusion

In this work, the successful deposition of electroless Ni–P–TiO_2 composite coatings on AH36 marine grade steel was achieved using leaf-mediated green synthesized TiO_2 nanoparticles from the *Indigofera tinctoria* extract. Anatase, rutile, and amorphous TiO_2 phases were formed through the green synthesis approach with their own structural and morphological features, which respectively play critical roles in improving the performance of coatings. The dispersion of such nanoparticles within the electroless plated Ni–P matrix led to uniform adherent coatings with high extent of microstructural refinement and improved functional attributes.

Out of the synthesized coatings, anatase-shielded sample (S3) presented greater coating thickness and microhardness due to higher surface energy and catalytic activity, as well as better dispersion stability in electrolyte. The effectiveness of the mixed-phase reinforcement was observed in hybrid coating (S4), which incorporated all three TiO_2 phases with the highest percentage, exhibited better surface uniformity, confirming the synergy resulting from composite doping. SEM and EDS analyses showed that the particles were evenly dispersed, with a stable microstructure of coating, while XRD analysis indicated the successful introduction of TiO_2 polymorphs into the Ni–P matrix.

- Polarization curves for the potentiodynamic polarization test indicated that the addition of TiO_2 to TCP improved corrosion resistance. The coatings containing rutile exhibited the lowest corrosion current density and highest positive corrosion potential, indicating that they have good passivation and barrier performance. The corrosion protection of anatase-reinforced coatings was better than that of pure Ni–P, and the corrosion resistance of amorphous TiO_2 was lower. The hybrid

TABLE 5 | Electrochemical corrosion parameters with corrosion rate.

Sample	TiO_2 phase	E_{corr} (V)	Log (I_{corr})	I_{corr} (A/cm^2)	Corrosion rate (mm/year)
Ni–P	None	−0.60	−6.2	6.3×10^{-7}	0.0074
Rutile	Rutile	−0.59	−7.8	1.6×10^{-8}	0.00019
Amorphous	Amorphous	−0.79	−5.0	1.0×10^{-5}	0.12
Anatase	Anatase	−0.70	−5.8	1.6×10^{-6}	0.019
Hybrid	Rutile + Amorphous + Anatase	−0.74	−4.9	1.25×10^{-5}	0.15

coating represented moderate corrosion resistance as a result of the collective action of various TiO_2 phases.

- The plant-based TiO_2 nanoparticles are efficient for the electroless Ni–P composite coatings as reinforcement materials, and they could be used environmentally friendly and high-performance options in marine structural applications. The fabricated coatings improve the hardness, surface characteristics, and corrosion resistance of AH36 steel, thus providing promising potential for protective applications in harsh marine conditions. Additional enhancements in terms of durability and long-term stability may be obtained with further optimization of particle dispersibility and phase compositions.

Conflicts of Interest

The authors declare no conflict of interest.

Data Availability Statement

Research data are not shared.

References

1. V. Krishnakumar and R. Elansezhian, "Wear and Corrosion Behavior of Electroless Ni-P-TiO_2-Al_2O_3 Nanocomposite Coatings on Magnesium AZ91D Alloy," *IOP Conference Series: Materials Science and Engineering* 912 (2020): 052020, https://doi.org/10.1088/1757-899X/912/5/052020.

2. W. Zhang, D. Cao, Y. Qiao, et al., "Microstructure and Properties of Duplex Ni-P-TiO_2/Ni-P Nanocomposite Coatings" *Materials Research* 22 (2019): 1–9, https://doi.org/10.1590/1980-5373-mr-2018-0748.

3. W. Liu, D. Sun, H. Ma, J. Huang, Z. Chen, and C. Gui, "Electroless Deposition to Fabricate Radiation Protection Suits for Pregnant Women: Effect of Water Bath Temperature on the Electromagnetic Shielding Performance," *ChemistrySelect* 6 (2021): 13409–13413, https://doi.org/10.1002/slct.202102961.

4. K. Shahzad, E. M. Fayyad, and M. Nawaz, et al., "Corrosion and Heat Treatment Study of Electroless NiP-Ti Nanocomposite Coatings Deposited on HSLA Steel," *Nanomaterials* 10 (2020): 1932, https://doi.org/10.3390/nano10101932.

5. A. Shozib, A. Ahmad, and M. S. A. Rahaman, et al., "Modelling and Optimization of Microhardness of Electroless Ni–P–TiO_2 Composite Coating Based on Machine Learning Approaches and RSM," *Journal of Materials Research and Technology* 12 (2021): 1010–1025, https://doi.org/10.1016/j.jmrt.2021.03.063.

6. R. A. S. Selvan, D. G. Thakur, M. Seeman, and M. Naik, "Surface Modification of AH36 Steel Using ENi-P-Nano TiO_2 Composite Coatings Through ANN-Based Modelling and Prediction," *Journal of Marine Science and Application* 21 (2022): 193–203, https://doi.org/10.1007/s11804-022-00288-5.

7. Z. Hao, Z. Zhang, and W. Zhou, et al., "Progress of Material Degradation: Metals and Polymers in Deep-Sea Environments," *Corrosion Reviews* 43 (2024): 315–334, https://doi.org/10.1515/corrrev-2024-0009.

8. M. Zhu, Y. Chen, Y. Chen, and K. Hu, "Application of Taguchi-Grey Relational Analysis for Optimizing Process Parameters of Laser Cladding for 316L Stainless Steel," *International Journal on Interactive Design and Manufacturing* 19 (2025): 6417–6428, https://doi.org/10.1007/s12008-024-02218-x.

9. M. Vijayanand, R. Varahamoorthi, P. Kumaradhas, S. Sivamani, and M. V. Kulkarni, "Regression-BPNN Modelling of Surfactant Concentration Effects in Electroless Ni B Coating and Optimization Using Genetic Algorithm," *Surface and Coatings Technology* 409 (2021): 126878, https://doi.org/10.1016/j.surfcoat.2021.126878.

10. I. U. Salicio-Paz, J. Sort, E. Pellicer, and E. García-Lecina, "Full Optimization of an Electroless Nickel Solution: Boosting the Performance of Low-Phosphorous Coatings," *Materials* 14 (2021): 1501, https://doi.org/10.3390/ma14061501.

11. S. Sarkar, R. K. Baranwal, R. Nandi, M. G. Dastidar, J. De, and G. Majumdar, "Parametric Optimization of Surface Roughness of Electroless Ni-P Coating," in *Optimization Methods in Engineering. Lecture Notes on Multidisciplinary Industrial Engineering*, ed. M. Tyagi, A. Sachdeva, and V. Sharma (Springer, 2021), 197–207.

12. K. Srivastwa, S. Sarkar, J. De, and G. Majumdar, "Parametric Optimization of Electroless Ni-P-CNT Coating Using Genetic Algorithm to Maximize the Rate of Deposition," *Materials Today: Proceedings* 66 (2022): 3769–3774, https://doi.org/10.1016/j.matpr.2022.06.106.

13. H. Nazari, G. B. Darband, and R. Arefinia, "A Review on Electroless Ni–P Nanocomposite Coatings: Effect of Hard, Soft, and Synergistic Nanoparticles," *Journal of Materials Science* 58 (2023): 4292–4358, https://doi.org/10.1007/s10853-023-08281-1.

14. E. M. Fayyad, A. M. Abdullah, M. K. Hassan, A. M. Mohamed, and G. Jarjoura, "Recent Advances in Electroless-Plated Ni-P and Its Composites for Erosion and Corrosion Applications: A Review," *Emergent Materials* 1 (2018): 3–24, https://doi.org/10.1007/s42247-018-0010-4.

15. S. A. Abde, L. Gawad, A. M. Baraka, and A. E. Morsi, "Development of Electroless Ni-P-Al_2O_3 and Ni-P-TiO_2 Composite Coatings From Alkaline Hypophosphite Gluconate Baths and Their Properties," *International Journal of Electrochemical Science* 8 (2013): 1722–1734, https://doi.org/10.1016/S1452-3981(23)14260-X.

16. R. Muraliraja, R. A. S. Selvan, and A. Selvakumar, et al., "A Review of Electroless Coatings on Non-Metals: Bath Conditions, Properties and Applications," *Journal of Alloys and Compounds* 960 (2023): 170723, https://doi.org/10.1016/j.jallcom.2023.170723.

17. F. Ali, M. Waseem, R. Khurshid, and A. Afzal, "TiO_2 Reinforced High-Performance Epoxy-co-Polyamide Composite Coatings," *Progress in Organic Coatings* 146 (2020): 105726, https://doi.org/10.1016/j.porgcoat.2020.105726.

18. H. Zhang, J. Zou, N. Lin, and B. Tang, "Review on Electroless Plating Ni–P Coatings for Improving Surface Performance of Steel," *Surface Review and Letters* 21 (2014): 1430002, https://doi.org/10.1142/S0218625X14300020.

19. M. Aravind, M. Amalanathan, and M. S. M. Mary, "Synthesis of TiO_2 Nanoparticles by Chemical and Green Synthesis Methods and Their Multifaceted Properties," *SN Applied Sciences* 3 (2021): 409, https://doi.org/10.1007/s42452-021-04281-5.

20. W. Chen, W. Gao, and Y. He, "A Novel Electroless Plating of Ni–P–TiO_2 Nano-Composite Coatings," *Surface and Coatings Technology* 204 (2010): 2493–2498, https://doi.org/10.1016/j.surfcoat.2010.01.032.

21. R. A. S. Selvan, D. G. Thakur, M. Seeman, R. Muraliraja, and M. I. Ansari, "Modelling and Optimisation of ENi-P-TiO_2 Coatings Synthesised With Zwitterionic Surfactant on Naval Grade AH36 Steel," *Sadhana* 47 (2022): 116, https://doi.org/10.1007/s12046-022-01890-7.

22. P. N. Birla, S. Arbuj, M. D. Shinde, et al., "Embedding Plasmonic Gold Nanoparticles in a ZnO Layer Enhanced the Performance of Inverted Organic Solar Cells Based on an Indacenodithieno[3,2-b]Thiophene-alt-5,5′-di(Thiophen-2-yl)-2,2′-Bithiazole-Based Push–Pull Polymer†," *RSC Advances* 13 (2023): 16175–16184.

23. P. Gadhari and P. Sahoo, "Effect of TiO_2 Particles on Micro-Hardness, Corrosion, Wear and Friction of Ni–P–TiO_2 Composite Coatings at Different Annealing Temperatures," *Surface Review and Letters* 23 (2015): 1550082, https://doi.org/10.1142/S0218625X15500821.

24. P. Gadhari and P. Sahoo, "Study of Hardness and Corrosion Resistance of Electroless Ni-P-TiO_2 Composite Coatings," *International Journal of Surface Engineering and Interdisciplinary Materials Science* 3 (2015): 18–40, https://doi.org/10.4018/IJSEIMS.2015070102.

25. O. Fayyaz, A. Khan, and R. A. Shakoor, et al., "Enhancement of Mechanical and Corrosion Resistance Properties of Electrodeposited Ni–P–TiC Composite Coatings," *Scientific Reports* 11 (2021): 5327, https://doi.org/10.1038/s41598-021-84716-6.

26. M. F. Achoi, M. N. Asiah, M. Rusop, and S. Abdullah, "Atomic Force Microscope (AFM) Studies of TiO_2 Nanocoated Glass Surface via Sol-Gel Coating," *Advanced Materials Research* 667 (2013): 128–134, https://doi.org/10.4028/www.scientific.net/AMR.667.128.